Identification of the limiting factors for high-temperature GaAs, GaInP, and AlGaInP solar cells from device and carrier lifetime analysis

E. E. Perl, D. Kuciauskas, J. Simon, D. J. Friedman, and M. A. Steiner

Citation: Journal of Applied Physics **122**, 233102 (2017);
View online: https://doi.org/10.1063/1.5003631
View Table of Contents: http://aip.scitation.org/toc/jap/122/23
Published by the American Institute of Physics

Identification of the limiting factors for high-temperature GaAs, GaInP, and AlGaInP solar cells from device and carrier lifetime analysis

E. E. Perl, D. Kuciauskas, J. Simon, D. J. Friedman, and M. A. Steiner
National Renewable Energy Laboratory, Golden, Colorado 80401, USA

(Received 6 September 2017; accepted 28 November 2017; published online 19 December 2017)

We analyze the temperature-dependent dark saturation current density and open-circuit voltage (V_{OC}) for GaAs, GaInP, and AlGaInP solar cells from 25 to 400 °C. As expected, the intrinsic carrier concentration, n_i, dominates the temperature dependence of the dark currents. However, at 400 °C, we measure V_{OC} that is ~50 mV higher for the GaAs solar cell and ~60–110 mV lower for the GaInP and AlGaInP solar cells compared to what would be expected from commonly used solar cell models that consider only the n_i^2 temperature dependence. To better understand these deviations, we measure the carrier lifetimes of p-type GaAs, GaInP, and AlGaInP double heterostructures (DHs) from 25 to 400 °C using time-resolved photoluminescence. Temperature-dependent minority carrier lifetimes are analyzed to determine the relative contributions of the radiative recombination, interface recombination, Shockley-Read-Hall recombination, and thermionic emission processes. We find that radiative recombination dominates for the GaAs DHs with the effective lifetime approximately doubling as the temperature is increased from 25 °C to 400 °C. In contrast, we find that thermionic emission dominates for the GaInP and AlGaInP DHs at elevated temperatures, leading to a 3–4× reduction in the effective lifetime and ~40× increase in the surface recombination velocity as the temperature is increased from 25 °C to 400 °C. These observations suggest that optimization of the minority carrier confinement layers for the GaInP and AlGaInP solar cells could help to improve V_{OC} and solar cell efficiency at elevated temperatures. We demonstrate V_{OC} improvement at 200–400 °C in GaInP solar cells fabricated with modified AlGaInP window and back surface field layers. *Published by AIP Publishing.*
https://doi.org/10.1063/1.5003631

I. INTRODUCTION

III-V materials have played an integral role in the advancement of a number of semiconductor technologies.[1,2] Nearly all light emitting and laser diodes are based on III-V materials due to the ability to combine a wide range of high quality materials with varying band structures into a single device.[3] The world's most efficient solar cells consist of multiple III-V semiconductor junctions and have achieved efficiencies above 45%, more than 1.5× higher than that of the best single junction configurations.[4–6] While the majority of these optoelectronic devices are designed to operate around room temperature, there are many applications that would benefit from the development of semiconductor devices that can operate at much higher temperatures. For example, developing solar cells that can maintain a relatively high efficiency at elevated temperatures could be an enabling technology for hybrid photovoltaic-thermal (PV-T) systems or near-sun space missions.[7–11] In addition to demonstrating outstanding reliability in harsh conditions, III-V materials have also exhibited very low voltage temperature coefficients.[12–14] These factors indicate that III-V materials could be the materials of choice for applications that require operation in a high-temperature environment. We recently demonstrated a dual-junction solar cell that maintained an efficiency above 15% at 400 °C with several pathways to improve the performance further.[15–18] In addition to the development of robust device components, such as a stable front metallization and cell encapsulation, a thorough understanding of the limiting factors at high-temperature is necessary for improving the device design.

II. EXPERIMENTAL

All of the solar cells and double heterostructures (DHs) in this study were grown at atmospheric pressure by organometallic vapor-phase epitaxy (OMVPE) using a custom-built vertical reactor on zinc-doped (001) GaAs substrates miscut 6° toward (111)A. Figure 1 shows the layer structure of the GaAs, GaInP, and AlGaInP solar cells analyzed in Sec. III, and includes the nominal thickness and the room-temperature bandgap of the semiconductor layers. All materials are lattice-matched to GaAs. Standard photolithography, electron-beam evaporation, and wet chemical etching techniques were used to process the samples into devices with an area of approximately 0.1 cm^2. Room-temperature Hall and capacitance-voltage measurements were taken to estimate the doping of the emitter ($N_D \approx 10^{18}\,cm^{-3}$) and base ($N_A \approx 10^{17}\,cm^{-3}$) layers. Additional details on the growth conditions and cell results can be found elsewhere.[15,19]

The DHs, analyzed later in Figs. 4 and 5, have a nominal thickness of 500 nm and have the same composition, growth conditions, and doping levels as the base layers of the solar cells shown in Fig. 1. The cladding layers of these structures have the same composition and are grown under the same conditions as the back surface field (BSF) layers of the initial

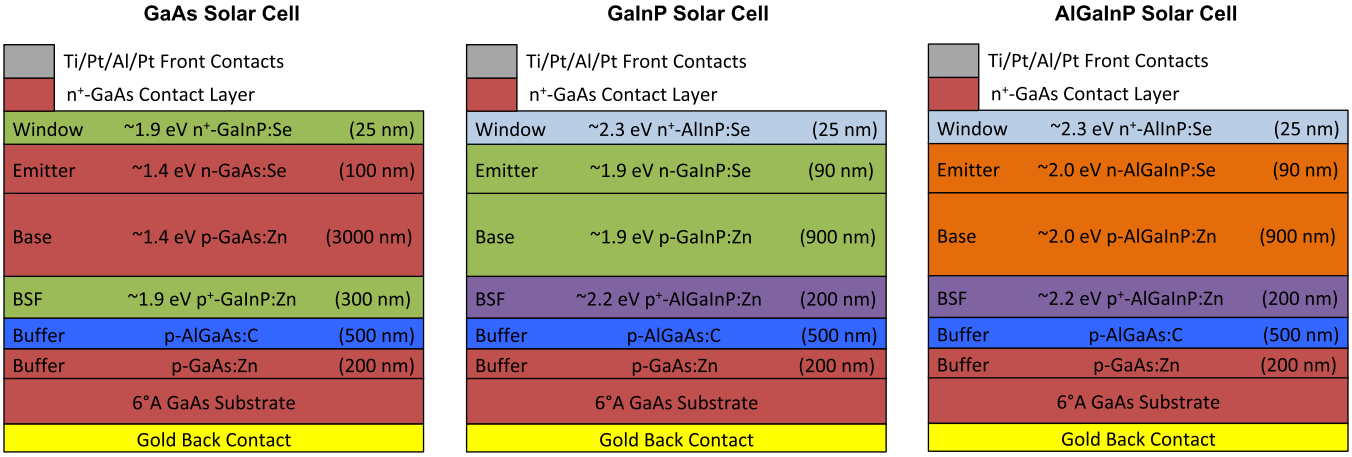

FIG. 1. Device schematic of the GaAs, GaInP, and AlGaInP solar cells showing the nominal room-temperature bandgaps, thicknesses, and the structure of the epitaxially grown layers. The diagram is not to scale.

set of solar cells. The nominal thickness of the GaInP DHs shown in Figs. 6 and 7 varies from 125 to 500 nm, but otherwise they are the same as the other GaInP DH.

To measure the solar cells and DHs at elevated temperatures, we use a temperature-controlled stage (Linkam HFS600E-PB4) capable of controlling the sample temperature from 25 to 600 °C. This stage is set up in conjunction with our existing current-voltage and flash testing setups to enable temperature-dependent measurements of the cells. Additional details are described elsewhere.[15] Charge carrier lifetimes were measured using time-resolved photoluminescence (TRPL).[20] Excitation was at 480 nm for the GaInP and AlGaInP DHs and 640 nm for the GaAs DHs with 300 fs pulses and a 1.1 MHz laser repetition rate. The excitation spot diameter was ≈0.3 mm, and the average excitation power was 0.4 mW. TRPL decays were measured at the maxima of the temperature-dependent emission bands by using appropriate bandpass interference filters. Time-correlated single photon counting with a silicon avalanche photodiode provided ≈0.02 ns time resolution, and deconvolution was not necessary in the data analysis. Exponential fits to TRPL data were used to determine minority carrier lifetimes measured in low-level injection conditions. A multimode optical fiber was used to deliver excitation pulses and to collect TRPL signals.[20]

III. DEVICE ANALYSIS

One approach to understand the device limitations is based on a dark current analysis of single-junction solar cells. The current-voltage (JV) characteristics of III-V solar cells frequently follow a two-diode model[21,22]

$$J = J_{01}\left(e^{q(V-JR_S)/kT}-1\right)+J_{0n}\left(e^{q(V-JR_S)/nkT}-1\right)+\frac{V-JR_S}{R_{Shunt}}-J_L, \tag{1}$$

where J is the current density, J_{01} is the dark saturation current density arising from recombination in the quasi-neutral regions, J_{0n} is the dark saturation current density arising from recombination in the depletion region and at the cell perimeter, n is the ideality factor associated with J_{0n}, q is the elementary charge, V is the applied voltage, k is the Boltzmann constant, T is the temperature, R_S is the series resistance, R_{Shunt} is the shunt resistance, and J_L is the photocurrent density. At high current densities, III-V solar cells are typically dominated by recombination in the quasi-neutral regions, a result of the larger exponent in the J_{01} term, and the J_{0n} factor will have a minimal impact on the cell voltage. At these high current densities, the open-circuit voltage (V_{OC}) can be approximated from the following equation:

$$V_{OC} = \frac{kT}{q} ln\left(\frac{J_L}{J_{01}}\right). \tag{2}$$

The analytical drift-diffusion model separates the J_{01} dark saturation current densities of a p-n junction into components corresponding to recombination in the n-type and p-type regions[21–23]

$$J_{01,nregion} = q\frac{n_i^2}{N_D}\sqrt{\frac{D_p}{\tau_p}}\left[\frac{\frac{S_pL_p}{D_p}\left(\cosh\left(\frac{x_n}{L_p}\right)\right)^2+\sinh\left(\frac{x_n}{L_p}\right)}{\frac{S_pL_p}{D_p}\sinh\left(\frac{x_n}{L_p}\right)+\cosh\left(\frac{x_n}{L_p}\right)}\right], \tag{3}$$

$$J_{01,pregion} = q\frac{n_i^2}{N_A}\sqrt{\frac{D_n}{\tau_n}}\left[\frac{\frac{S_nL_n}{D_n}\left(\cosh\left(\frac{x_p}{L_n}\right)\right)^2+\sinh\left(\frac{x_p}{L_n}\right)}{\frac{S_nL_n}{D_n}\sinh\left(\frac{x_p}{L_n}\right)+\cosh\left(\frac{x_p}{L_n}\right)}\right], \tag{4}$$

where n_i is the intrinsic carrier concentration, N_D is the donor concentration in the n-type region, N_A is the acceptor concentration in the p-type region, D_p is the minority carrier diffusion coefficient for holes, D_n is the minority carrier diffusion coefficient for electrons, τ_p is the minority carrier lifetime for holes, τ_n is the minority carrier lifetime for electrons, S_p is the surface recombination velocity for minority holes, S_n is the surface recombination velocity for minority electrons, L_p is the minority carrier diffusion length for

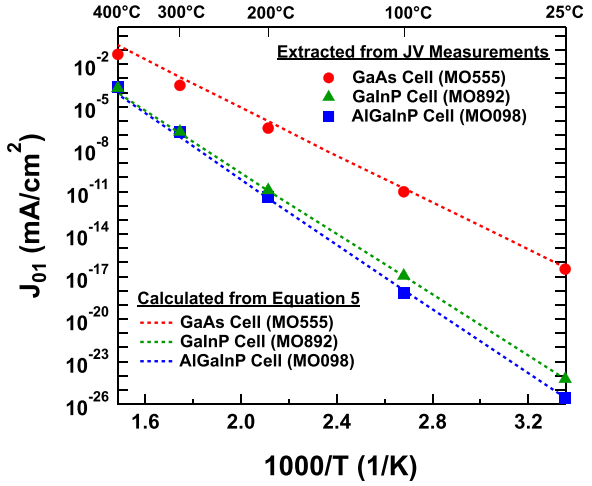

FIG. 2. Comparison between measured and modeled J_{01} dark saturation current densities for GaAs, GaInP, and AlGaInP solar cells. The markers show the J_{01} dark saturation current densities extracted from temperature-dependent JV measurements, and the dashed lines show the J_{01} dark saturation current densities calculated from Eq. (5). The calculated J_{01} dark saturation current densities are adjusted for agreement at 25 °C.

holes, L_n is the minority carrier diffusion length for electrons, x_n is the thickness of the n-type region, and x_p is the thickness of the p-type region. By far, the most important impact of increasing the temperature is the exponential increase in the intrinsic carrier concentration, n_i, which in turn leads to an exponential rise in the J_{01} dark saturation current densities and consequently a drop in the V_{OC} of a solar cell. The temperature dependence of the n_i^2 factor in Eqs. (3) and (4) can be described by the following proportionality, where E_g is the bandgap:

$$n_i{}^2 \propto T^3 e^{-E_g(T)/kT}. \tag{5}$$

To test the validity range of this model, we grew single-junction GaAs ($E_{g,25\,^\circ C} \approx 1.4$ eV), GaInP ($E_{g,25\,^\circ C} \approx 1.9$ eV), and AlGaInP ($E_{g,25\,^\circ C} \approx 2.0$ eV) solar cells, as shown in Fig. 1.

We extract J_{01} for the GaInP and AlGaInP cells by fitting dark JV measurements to Eq. (1) and observe a clear n = 1 region above ~10 mA/cm^2 for all temperatures between 25 and 400 °C. For the GaAs solar cell, we are unable to fit dark JV measurements to the n = 1 line at the highest temperatures due to series resistance effects and instead extract J_{01} from concentrator measurements. Additional details are reported elsewhere.[15,19] The markers in Fig. 2 show the temperature-dependent J_{01} dark saturation current densities extracted from JV measurements, while the dashed lines show the J_{01} dark saturation current densities calculated from the proportionality of Eq. (5), adjusted for agreement at room temperature.

It is clear from these plots that the n_i^2 factor dominates the J_{01} temperature dependence, driving a ~15–22 order-of-magnitude increase in J_{01} for the three cells as the temperature is increased from 25 °C to 400 °C. Since n_i is the dominant factor, solar cell models often make the simplifying assumption that the other factors in Eqs. (3) and (4) are constant with temperature.[16,24–26] At the highest temperatures, however, the data deviate slightly from the model, as can be seen on the left in Fig. 2. This deviation is clearer when considering V_{OC}.

In Fig. 3, the solid markers show V_{OC} at a photocurrent density of 5 A/cm^2 (~500 suns) for the GaAs, GaInP, and AlGaInP solar cells as measured using a High Intensity Pulsed Solar Simulator (HIPSS).[27] The solid lines represent the expected temperature-dependence of V_{OC} from Eqs. (2) and (5), where the J_{01} dark saturation current densities are again adjusted for agreement at 25 °C. For the GaInP cell, we also include data showing V_{OC} calculated from Eq. (2) but using the J_{01} dark saturation current densities that were extracted from dark JV measurements, and the results from this technique are in good agreement with the HIPSS data. Based on repeated measurements of single-junction solar cells at the same light intensity, we observe a variation of less than 10 mV in V_{OC} on the HIPSS.

Equations (2) and (5) give a reasonable approximation of V_{OC} at elevated temperatures, but we still measure >50 mV deviation in V_{OC} from these analytical models. For the GaAs cell, the measured V_{OC} is higher than the model, while for the GaInP and AlGaInP cells, the measured V_{OC} is lower. To understand these deviations, we reconsider the validity of the underlying assumption that only the temperature dependence of n_i is significant.

IV. CARRIER LIFETIME ANALYSIS

To investigate the temperature dependence of the other factors in Eqs. (3) and (4), we study the carrier lifetimes of

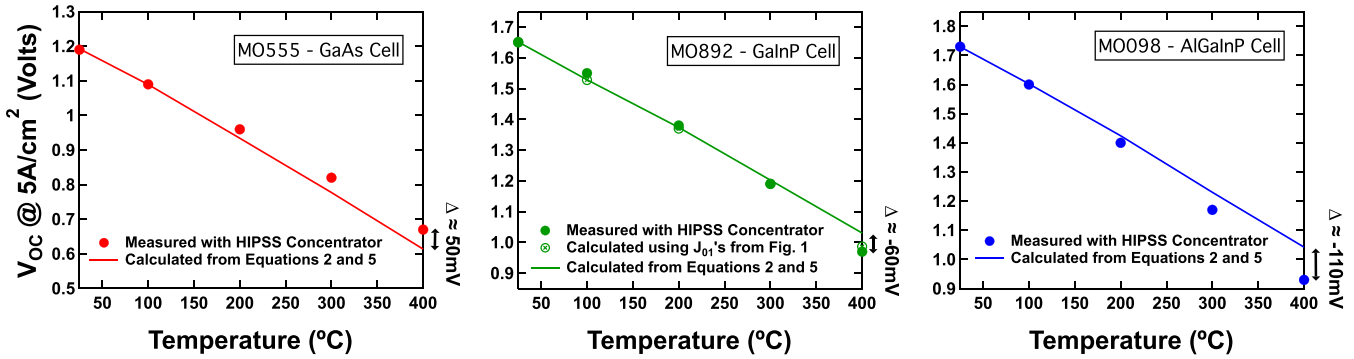

FIG. 3. Temperature dependence of V_{OC} at a photocurrent of 5 A/cm^2 (~500 suns) for GaAs, GaInP, and AlGaInP solar cells are measured using the HIPSS (solid markers) and are calculated from Eqs. (2) and (5) (lines). For the GaInP cell, we also include data showing V_{OC} calculated from Eq. (2) but using the J_{01} dark saturation current densities that were extracted from dark JV measurements (open markers).

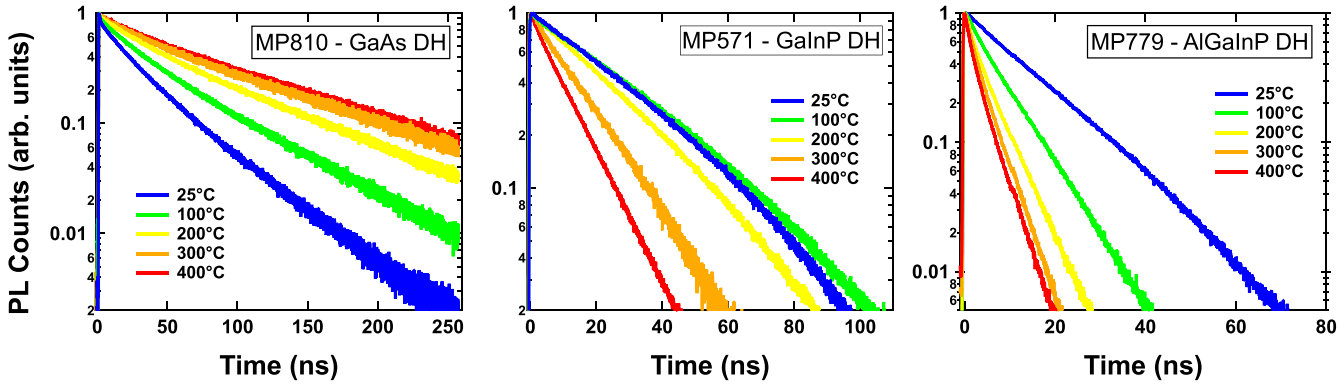

FIG. 4. Normalized TRPL decay curves for GaAs, GaInP, and AlGaInP DHs measured at 25–400 °C. At elevated temperatures, we observe longer effective TRPL lifetimes for the GaAs DH and shorter effective TRPL lifetimes for the GaInP and AlGaInP DHs.

p-type GaAs, GaInP, and AlGaInP DHs. Figure 4 shows the normalized decay curves for the GaAs, GaInP, and AlGaInP DHs at 25–400 °C.

We observe that the TRPL decays of the GaAs DH are slower at elevated temperatures, but we see the opposite trend for the GaInP and AlGaInP DHs.[28–30] This is consistent with the temperature dependences of V_{OC} in Fig. 3. In other words, a GaAs solar cell with an effective lifetime that increases at higher temperature would have a lower J_{01} and higher V_{OC} than we would expect from Eqs. (2) and (5). Similarly, a GaInP or an AlGaInP solar cell with a lifetime that decreases at higher temperature would have a higher J_{01} and lower V_{OC} than we would expect from Eqs. (2) and (5).

Temperature-dependent lifetimes, extracted from the decay curves of Fig. 4, are fit to a recombination model to determine the relative contributions of the radiative recombination (lifetime τ_{rad}), Shockley-Read-Hall recombination (lifetime τ_{SRH}), interface recombination (lifetime τ_{int}), and thermionic emission (lifetime τ_{th}) processes. Here, τ_{int} refers to the recombination of carriers due to traps at the interface between the absorber and barrier layers, whereas τ_{th} refers to the thermal escape of carriers over the barrier. The Shockley-Read Hall and interface lifetimes have the same temperature dependence and are thus considered together. The analytical descriptions for the temperature dependences of τ_{rad}, τ_{SRH}, τ_{int}, and τ_{th} are described in the literature.[31,32]

For the analysis of our data, the temperature dependences of these lifetimes can be simplified as[33]

$$\tau_{rad} \propto C_{rad} \mathrm{T}^{1.5}, \tag{6}$$

$$\tau_{SRH,int} \propto C_{SRH,int} \mathrm{T}^{-0.5}, \tag{7}$$

$$\tau_{th} \propto C_{th} \mathrm{T}^{-0.5} * e^{\Delta \mathrm{E}/kT}, \tag{8}$$

where ΔE is the effective barrier height and C_{rad}, $C_{SRH,int}$, and C_{th} are temperature-independent proportionality constants for the radiative recombination, Shockley-Read-Hall recombination,[32] interface recombination, and thermionic emission processes, respectively.[31,33] The effective recombination rate, $1/\tau_{eff}$, includes all recombination pathways

$$\frac{1}{\tau_{eff}} = \frac{1}{\tau_{rad}} + \frac{1}{\tau_{SRH}} + \frac{1}{\tau_{int}} + \frac{1}{\tau_{th}}. \tag{9}$$

The markers in Fig. 5 show the effective carrier lifetimes measured by TRPL as a function of temperature for the GaAs, GaInP, and AlGaInP DHs. The dashed lines in Fig. 5 indicate fitting results of the data to Eqs. (6)–(9). The GaAs DH is dominated by radiative recombination, with only a small contribution from the other terms at the highest temperatures. This drives a ∼2.5× increase in the effective lifetime as the temperature is increased from 25 °C to 400 °C. While the

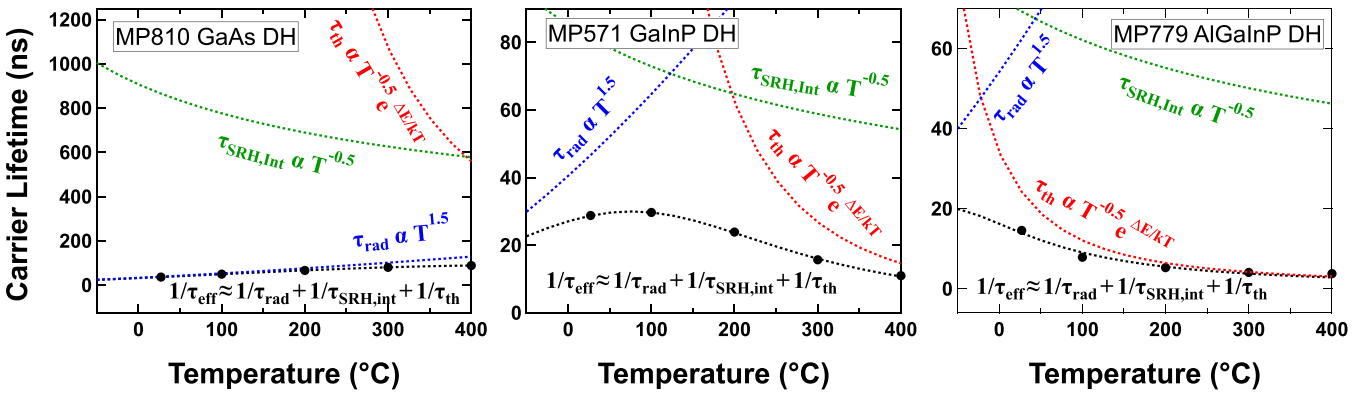

FIG. 5. Measured carrier lifetime temperature dependence for GaAs, GaInP, and AlGaInP DHs (solid markers). The dashed lines indicate fitting results for τ_{eff} (black), τ_{rad} (blue), $\tau_{SRH,int}$ (green), and τ_{th} (red). Note the difference in the vertical scales between the three graphs.

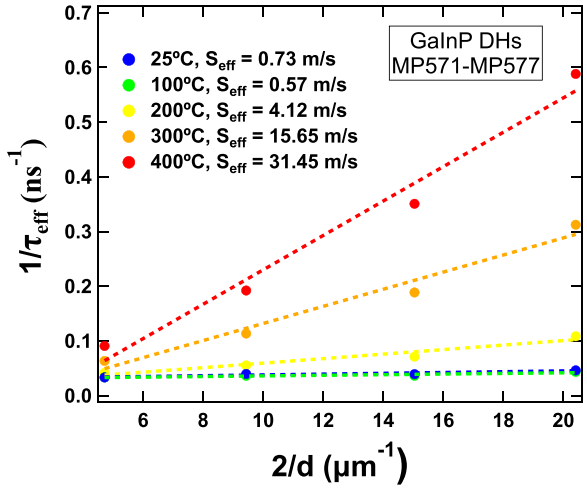

FIG. 6. Plots of the inverse effective lifetime versus inverse sample thickness, 2/d, for GaInP DHs. S_{eff}(T) is extracted from the slope of each curve.

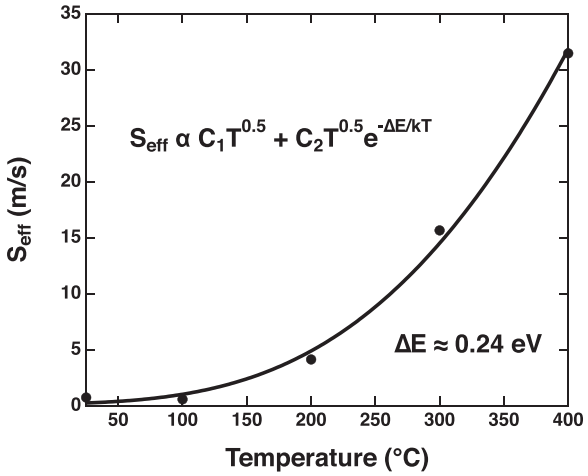

FIG. 7. Plots of S_{eff}(T) for GaInP double heterostructures (solid markers). A fit of this data to Eq. (11) is also shown (solid line), allowing us to extract a value of 0.24 eV for ΔE.

radiative lifetime is dominant for the GaInP DH at 25 °C, the other recombination mechanisms quickly overtake it as the temperature is increased, and thermionic emission becomes dominant above ∼200 °C. This drives a ∼3× decrease in the effective lifetime at 400 °C. For the AlGaInP DH, thermionic emission is dominant at all temperatures, and this drives a ∼4× decrease in the effective lifetime as the temperature is increased from 25 °C to 400 °C.

Next, we consider the surface recombination. Assuming that the interface recombination and thermionic emission processes can be parameterized by recombination velocities, the effective surface recombination velocity (S_{eff}) can be taken as the sum of the interface recombination velocity (S_{int}) and thermionic emission recombination velocity (S_{th}), and Eq. (9) for the effective lifetime τ_{eff} can be re-expressed in terms of S_{eff}[34]

$$\frac{1}{\tau_{eff}} = \frac{1}{\tau_{rad}} + \frac{1}{\tau_{SRH}} + \frac{2S_{eff}}{d}, \tag{10}$$

where d is the thickness of the DH.[33,35] This analysis is most important for the GaInP DH, where we observe the transition from the radiative recombination to the Shockley-Read-Hall recombination to the thermionic emission [Fig. 5(b)]. To determine the temperature dependence of S_{eff}, we grew four GaInP DHs of varying thickness (nominally 125–500 nm). More accurate thicknesses for the DHs were determined from the interference fringes of a 632 nm laser reflecting off the epilayer surface during growth. Effective lifetimes were determined for these DHs at 25–400 °C using TRPL. Plots of $1/\tau_{eff}$ versus 2/d are shown in Fig. 6, with linear fits to the data shown as dashed lines. S_{eff} can be determined from the slope of these curves, as is evident from Eq. (10).[29]

We observe a ∼40× increase in S_{eff} as the temperature is increased from 25 °C to 400 °C. The relative contribution from S_{int} and S_{th} can be deconvolved by fitting these data to Eqs. (7)–(10),

$$S_{eff} = \frac{d}{2\tau_{int}} + \frac{d}{2\tau_{th}} = C_1 T^{0.5} + C_2 T^{0.5} e^{-\Delta E/kT}. \tag{11}$$

Here, C_1 and C_2 are temperature independent proportionality constants. Figure 7 shows a fit of S_{eff}(T) to Eq. (11), where the values for S_{eff} are taken from Fig. 6.

The fits are entirely dominated by the exponential function in the thermionic emission term, and we are able to extract a barrier height for minority electrons at the GaInP/AlGaInP interface, $\Delta E = 0.24 \pm 0.01$ eV, very close to what we expect for these two materials.

V. DISCUSSION

Given the uncertainties in the modeling and measurement, and the fact that the solar cells have both n-side and p-side effects whereas the DH experiments were only on p-type samples, it is not possible to directly apply the measured DH lifetimes to Eqs. (3) and (4). The carrier lifetime analysis will, however, allow us to approximate the impact of the temperature-dependent lifetimes on V_{OC}. For the GaAs DH, τ_{rad} dominates the minority carrier lifetime across the entire temperature range and drives a ∼2.5× increase in the bulk lifetime as the temperature is increased to 400 °C. Since the bulk lifetime shows up in the denominator of Eqs. (3) and (4), we would expect τ_{rad} to drive a ∼1.5× decrease in J_{01} relative to Eq. (5), and this will lead to a ∼30 mV increase in V_{OC} at 400 °C for a GaAs solar cell compared to Eqs. (2) and (5). The increasing bulk lifetime makes up a significant fraction of the deviation that we observe in Fig. 3. Note that our carrier lifetime analysis was for p-type DHs, but we expect similar conclusions for n-type DHs based on the bandgaps and band offsets.

Next, we analyze the potential to increase V_{OC} of GaInP solar cells based on our findings that at elevated temperatures, the effective lifetime is dominated by thermionic emission. An analysis of the impact of S_{eff} on V_{OC} of a solar cell is reported in Ref. 23, and it is shown that the ∼40× increase in S_{eff} that we observe as the temperature is increased from 25 °C to 400 °C can reduce V_{OC} by ∼100 mV in the expected operating regime of our solar cells where the thickness exceeds the diffusion length and $0.01 < \frac{SL}{D} < 100$.

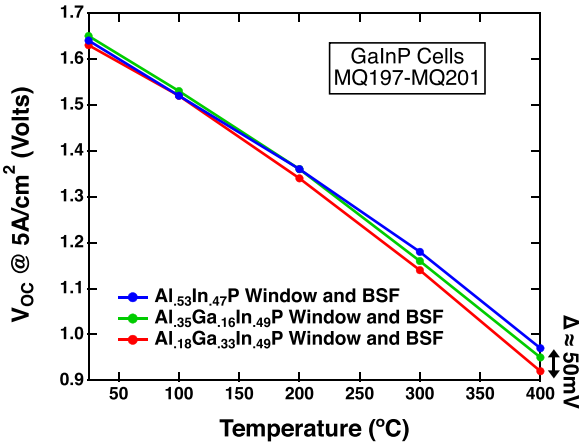

FIG. 8. Temperature dependence of V_{OC} at a photocurrent of 5 A/cm^2 (~500 suns) for GaInP solar cells with varying window layers and BSF compositions.

We are able to explore the significance of the passivation layers on $V_{OC}(T)$ experimentally by growing GaInP solar cells with different minority carrier confinement layers. For this study, we grew three GaInP solar cells with varying aluminum compositions for the AlGaInP window and back surface field (BSF) layers. The nominal aluminum compositions of these layers are 18% ($Al_{0.18}Ga_{0.33}In_{0.49}P$, $E_{g,25\,^\circ C} \approx 2.1$ eV), 35% ($Al_{0.35}Ga_{0.16}In_{0.49}P$, $E_{g,25\,^\circ C} \approx 2.2$ eV), and 53% ($Al_{0.53}In_{0.47}P$, $E_{g,25\,^\circ C} \approx 2.3$ eV) based on calibrations of the growth reactor. Figure 8 shows the temperature dependence of V_{OC} at a photocurrent density of 5 A/cm^2 for these three samples as measured using the HIPSS.

While we measure a similar V_{OC} for each sample at room temperature, we begin to see the expected divergence in V_{OC} as thermionic emission overtakes the other recombination mechanisms. At 400 °C, V_{OC} increases by ~50 mV when the bandgap of the minority carrier confinement layers is increased by ~200 meV. These results indicate that additional efforts to improve the design of the minority carrier confinement layers could notably improve the performance of a GaInP or AlGaInP solar cell at elevated temperatures. It is important to note, however, that there is a significant challenge in further reducing the effect of thermionic emission for a GaInP or AlGaInP solar cell because material constraints limit the bandgap of a lattice-matched III-V cladding layer to less than ~2.3 eV ($Al_{0.53}In_{0.47}P$). For GaAs solar cells, however, these materials can be used as effective barriers, and the data presented in Figs. 3 and 5 indicate that the barrier remains effective even at temperatures as high as 400 °C.

VI. CONCLUSIONS

In summary, we analyze the J_{01} dark saturation current densities and V_{OC} of GaAs, GaInP, and AlGaInP solar cells from 25 to 400 °C. While the intrinsic carrier concentration dominates the temperature dependence of J_{01}, we measure V_{OC} for the GaAs solar cell that is higher and V_{OC} for the GaInP and AlGaInP solar cells that are lower than we would expect from commonly used solar cell models that consider only the n_i^2 temperature dependence. To better understand these deviations, we analyze the carrier lifetime of GaAs, GaInP, and AlGaInP DHs from 25 to 400 °C using TRPL. We find that the performance of the GaAs DH is dominated by radiative recombination at all temperatures and this drives an increase in the effective lifetime at high temperatures. On the other hand, carrier lifetimes in the GaInP and AlGaInP DHs are dominated by thermionic emission and this leads to a 3–4× reduction in the carrier lifetime as the temperature is increased from 25 °C to 400 °C. In this temperature range, the surface recombination velocity for the GaInP correspondingly increases by ~40×. The lower effective lifetime and higher surface recombination velocity can explain why V_{OC} of the GaInP and AlGaInP solar cells are lower than predicted by the n_i^2 temperature dependence of J_{01}. These studies indicate that additional efforts to improve the design of the minority carrier confinement layers for GaInP and AlGaInP solar cells could help to improve V_{OC} and efficiency at elevated temperatures, although material constraints place a practical limitation on the achievable barrier height for III-V materials lattice-matched to GaAs.

ACKNOWLEDGMENTS

The authors are pleased to thank W. Olavarria, M. Young, and C. Beall at NREL for processing work. We would also like to thank Minjoo Larry Lee and John Geisz for useful conversations. This work was supported by the U.S. Department of Energy through the ARPA-E FOCUS program under Award No. DE-AR0000508 and through Contract No. DE-AC36-08GO28308 with the National Renewable Energy Laboratory. The U.S. Government retains, and the publisher by accepting the article for publication acknowledges that the U.S. Government retains, a nonexclusive, paid up, irrevocable, worldwide license to publish or reproduce the published form of this work, or allow others to do so, for U.S. Government purposes.

[1]S. Mokkapati and C. Jagadish, Mater. Today **12**(4), 22 (2009).
[2]S. M. Sze, *Semiconductor Devices: Physics and Technology* (John Wiley & Sons, 2008).
[3]E. F. Schubert, T. Gessmann, and J. K. Kim, *Light Emitting Diodes* (John Wiley & Sons, Inc., 2005).
[4]M. A. Green, Y. Hishikawa, W. Warta, E. D. Dunlop, D. H. Levi, J. Hohl-Ebinger, and A. W. Ho-Bailie, Prog. Photovoltaics: Res. Appl. **25**(7), 668 (2017).
[5]F. Dimroth, T. N. D. Tibbits, M. Niemeyer, F. Predan, P. Beutel, C. Karcher, E. Oliva, G. Siefer, D. Lackner, P. Fuß-Kailuweit, and A. W. Bett, IEEE J. Photovoltaics **6**(1), 343 (2016).
[6]R. M. France, J. F. Geisz, I. Garcia, M. A. Steiner, W. E. McMahon, D. J. Friedman, T. E. Moriarty, C. Osterwald, J. S. Ward, A. Duda, and M. Young, IEEE J. Photovoltaics **5**(1), 432 (2015).
[7]H. M. Branz, W. Regan, K. J. Gerst, B. B. Borak, and E. A. Santoria, Energy Environ. Sci. **8**, 3083 (2015).
[8]T. T. Chow, Appl. Energy **87**(2), 365 (2010).
[9]Y. Vorobiev, J. González-Hernández, P. Vorobiev, and L. Bulat, Sol. Energy **80**(2), 170 (2006).
[10]G. A. Landis, D. Merritt, R. P. Raffaelle, and D. Scheiman, paper presented at the 18th Space Photovoltaic Research and Technology Conference, 2005.
[11]O. V. Sulima, P. E. Sims, J. A. Cox, M. G. Mauk, R. L. Mueller, R. C. Reedy, A. M. Khammadov, P. D. Paulson, and G. A. Landis, paper presented at the Proceedings of 3rd World Conference on Photovoltaic Energy Conversion, 2003.
[12]C. Algora, *Handbook on Concentrator Photovoltaic Technology* (John Wiley & Sons, 2016).

[13]A. Virtuani, D. Pavanello, and G. Friesen, in *5th World Conference on Photovoltaic Energy Conversion* (2010), p. 6.
[14]M. A. Steiner, J. F. Geisz, D. J. Friedman, W. J. Olavarria, A. Duda, and T. E. Moriarty, paper presented at the 37th Photovoltaic Specialists Conference, Seattle, 2011.
[15]E. E. Perl, J. Simon, J. F. Geisz, M. L. Lee, D. J. Friedman, and M. A. Steiner, IEEE J. Photovoltaics **6**(5), 1345 (2016).
[16]D. J. Friedman, M. A. Steiner, E. E. Perl, and J. Simon, paper presented at the 44th IEEE Photovoltaic Specialists Conference, Washington, DC, 2017.
[17]M. A. Steiner, E. E. Perl, J. Simon, D. J. Friedman, N. Jain, P. Sharps, C. McPheeters, and M. L. Lee, AIP Conf. Proc. **1881**(1), 040007 (2017).
[18]M. A. Steiner, E. E. Perl, J. Simon, D. J. Friedman, N. Jain, P. Sharps, C. McPheeters, and M. L. Lee, paper presented at the 44th IEEE Photovoltaics Specialists Conference, Washington, DC, 2017.
[19]E. E. Perl, J. Simon, J. F. Geisz, W. Olavarria, M. Young, A. Duda, D. J. Friedman, and M. A. Steiner, IEEE J. Photovoltaics **6**(3), 770 (2016).
[20]D. Kuciauskas, J. N. Duenow, J. V. Li, M. R. Young, P. Dippo, and D. H. Levi, paper presented at the Proceedings of the 38th IEEE Photovoltaic Specialist Conference, Austin, TX, 2012.
[21]A. L. Fahrenbruch and R. H. Bube, *Fundamentals of Solar Cells Photovoltaic Solar Energy Conversion* (Academic Press, new York, 1983).
[22]H. J. Hovel, *Solar Cells* (Academic Press, New York, 1975).
[23]S. R. Kurtz, J. M. Olson, D. J. Friedman, J. F. Geisz, A. E. Kibbler, and K. A. Bertness, in *MRS Spring Meeting* (San Francisco, CA, 1999).
[24]D. J. Friedman, paper presented at the 25th IEEE Photovoltaic Specialists Conference, Washington D.C., 1996.
[25]J. C. Fan, Sol. Cells **17**, 309 (1986).
[26]M. Ochoa, M. A. Steiner, I. García, J. F. Geisz, D. J. Friedman, and C. Algora, Prog. Photovoltaics: Res. Appl. **24**(3), 357 (2016).
[27]K. Emery, M. Meusel, R. Beckert, F. Dimroth, A. Bett, and W. Warta, paper presented at the 28th IEEE Photovoltaic Specialists Conference, Anchorage, Alaska, 2000.
[28]J. P. Bergman, C. Hallin, and E. Janzen, J. Appl. Phys. **78**(7), 4808 (1995).
[29]J. M. Olson, R. K. Ahrenkiel, D. J. Dunlavy, B. Keyes, and A. E. Kibbler, Appl. Phys. Lett. **55**(12), 1208 (1989).
[30]F. J. Schultes, T. Christian, R. Jones-Albertus, E. Pickett, K. Alberi, B. Fluegel, T. Liu, P. Misra, A. Sukiasyan, and H. Yuen, Appl. Phys. Lett. **103**(24), 242106 (2013).
[31]H. Schneider and K. V. Klitzing, Phys. Rev. B **38**(9), 6160 (1988).
[32]Y. Rosenwaks, I. Tsimberova, H. Gero, and M. Molotskii, Phys. Rev. B **68**, 115210 (2003).
[33]S. Liu, X. H. Zhao, C. M. Campbell, M. B. Lassise, Y. Zhao, and Y. H. Zhang, Appl. Phys. Lett. **107**(4), 041120 (2015).
[34]R. K. Ahrenkiel, *Minority Carriers in III - V Semiconductors: Physics and Applications*, edited by R. K. Ahrenkiel and M. S. Lundstrom (Academic Press Inc., San Diego, CA, 1993), Vol. 39, p. 39.
[35]M. A. Steiner, J. F. Geisz, I. Garcìa, D. J. Friedman, A. Duda, W. Olavarria, M. Young, and S. R. Kurtz, J. Photovoltaics **3**, 1437 (2013).